INL/JOU-22-65791-Revision-0

Rate-dependent dynamic cylindrical cavity expansion equations for conical- and ogival-nosed projectiles

August 2022

Changing the World's Energy Future

Zherui Guo

Idaho National Laboratory

INL/JOU-22-65791-Revision-0

Rate-dependent dynamic cylindrical cavity expansion equations for conical- and ogival-nosed projectiles

Zherui Guo

August 2022

Idaho National Laboratory
Idaho Falls, Idaho 83415

http://www.inl.gov

Prepared for the
U.S. Department of Energy
Under DOE Idaho Operations Office
Contract DE-AC07-05ID14517

Rate-dependent dynamic cylindrical cavity expansion equations for conical- and ogival-nosed projectiles

Zherui Guo[*1]

*Corresponding author
Zherui Guo
Tel.: +1 (208) 526-3607.
E-mail address: Zherui.Guo@inl.gov
ORCiD: 0000-0002-8832-8435

[1]Idaho National Laboratory, Idaho Falls, ID, USA

Abstract

The dynamic cylindrical cavity expansion model for a rate-dependent target material was previously derived by Warren to examine the effects of strain-rate sensitivity on the radial stress acting on a perforating projectile. However, the equations presented were largely analytical and were not further applied to predict the ballistic performance of ductile target plates. The current work expands on Warren's derivation to model the dynamics of conical and ogival geometries, and the rate-dependent model is compared to prior experimental results of 7.62-mm APM2 rounds impacting 6061-T6511 aluminum alloy plates. Results show that including rate effects improves the ballistic performance prediction, even for a marginally strain-rate sensitive material such as Al6061-T651. However, existing semi-empirical variations of the cavity expansion model can provide the same degree of accuracy if target material rate-sensitivity parameters are not readily available.

Keywords: Ballistic impact. Cavity expansion. Strain-rate sensitivity. Plate perforation.

Introduction

In an early series of works [1–4], Forrestal and colleagues derived cylindrical cavity expansion (CCE) equations to model the dynamic response of rate-independent, strain-hardening target plates under ballistic impact. In the CCE model, the target plate is idealized as infinitesimally thin layers (i.e. plane strain conditions) perpendicular to the direction of projectile perforation. A set of closed-form equations were then derived [5] to predict the ballistic performance of aluminum target plates against ogival- and conical-nosed long rod projectiles at normal incidence impact using the rate-independent CCE model. Subsequent works [6–12] used a semi-empirical variation of the CCE model to successfully predict the ballistic impact performance aluminum and steel plates impacted by armor-piercing rounds.

In a parallel series of works, Forrestal et al. derived closed-form spherical cavity-expansion (SCE) equations for long rods penetrating deep metallic targets [13–15]. In contrast to plate perforation dynamics, which can be accurately described by CCE models, deep target penetration dynamics are more accurately represented by SCE models. Earlier SCE formulations assumed rate-insensitivity of the target materials, and the depth of penetration results were well-predicted for aluminum targets. Warren & Forrestal [16] later developed closed-form SCE models for the deep target penetration of rate-dependent materials (rSCE).

Following the rSCE model, Warren [17] then derived cylindrical cavity expansion equations for rate-dependent materials (rCCE). While the radial expansion stress was shown to increase as a result of rate effects, the rCCE model itself was not applied to predict the results of ballistic perforation experiments.

In this work, equations for the rCCE model are derived and applied to the ballistic perforation of ductile target plates. The rate-independent CCE equations are presented in the first section to form a basis for analysis, before rate effects (as derived by Warren) are included in the subsequent section. Equations are then derived for the target resistive forces acting on generic conical- and ogival-nosed projectiles, before model predictions are presented for 7.62-mm APM2 rounds impacting 6061-T6511 aluminum alloy plates. Different variations of the cylindrical cavity expansion model are compared to ballistic experimental results to explain the success of semi-empirical model predictions as demonstrated in previous works.

Derivation of model equations

Rate-independent cylindrical cavity expansion (CCE)

The stress-strain law for a typical strain-hardening material is given by the modified Ludwik equation

(1)

In Equation 1, σ is the true stress, E is the target elastic modulus, ε is true strain, Y is the quasi-static target yield stress, and n is a strain-hardening exponent obtained from fitting Equation 1 to quasi-static uniaxial compression test data to high strains greater than 1.0 [18]. The exact solution for the radial stress σ_r at the cavity surface when expanding radially with velocity V is the sum of two loading responses: quasi-static strain hardening and target inertia.

(2)

(3)

(4)

In Equations 2 to 4, ρ_t is the target density, v is the Poisson's ratio, and B is a target radial inertia given by

(5)

(6)

Since B is velocity-dependent, an empirical parameter B_0 is usually curve-fitted so that a closed-form solution may be obtained as [3]

(7)

Assuming a frictionless perforation process [5], the perforation dynamics can be modeled with the solution of the differential equation

(8)

where z is the penetration depth, V_z the axial velocity, and m_p is the projectile mass given as

(9a)

(b)

with a being the projectile radius, ρ_p the projectile density, L the projectile shank length, k_1 the nose shape factor, and the projectile nose length. From Ref. [5], the axial force F_z acting on the projectile nose is given as

(10)

N is a dimensionless nose shape factor dependent on the target inertia, the derivation of which will be expanded upon in subsequent sections. Solution of Equations 8 to 10 gives

(11)

The ballistic limit velocity V_{bl} is obtained by integrating the perforation depth from to the plate thickness , and the perforation velocity V_z from to .

(12a)

(b)

(c)

For a striking velocity V_s above the ballistic limit V_{bl}, the residual velocity V_r can be calculated by integrating V_z from to in Equation 12 to give

(13)

(14)

Multiplying Equation 12c by and substituting into Equation 14, the residual velocity can be explicitly expressed as a function of V_s and V_{bl}

(15)

From Equation 12a, C is a dimensionless term related to the inertia of the target material via B_0 in Equation 7. A three-term series approximation for the exponential terms in Equations 12c and

15 gives

(16)

(17)

These series approximations allow for the inertial effects via the C term to be easily excluded for certain materials where target inertia is negligible during the perforation process. Prior studies often excluded the effects of target inertia in Equation 16 [5,19], but instead used an empirical constant κ for ballistic performance prediction such that

(18)

Rate-dependent cylindrical cavity expansion (rCCE)

Warren & Forrestal [16,17] subsequently derived a strain-rate sensitive perforation model, starting with a rate-decoupled stress-strain law [20,21]:

(19)

(20)

In Equations 19 and 20, Y_d is the dynamic yield stress of the target material. The rate-sensitivity modification to the post-yield stress consists of a curve-fitted rate parameter α, reference strain-rate , and strain-rate sensitivity exponent β. When $\alpha = 0$, the rate-independent modified Ludwik equation (Equation 1) is recovered. The exact solution for the rate-dependent radial stress is now the sum of three loading responses: quasi-static strain hardening, target inertia, and strain-rate sensitivity. The equations are given as

(21)

(22)

(23)

where R_c is the cavity radius, usually taken as the projectile shank radius for the cylindrical cavity expansion model. The subscript R indicates rate-dependent forms of the variable. Warren showed that strain rate effects have a negligible influence on the strain-hardening portion of the stress-strain curve [17]. Therefore, Equation 22 can be approximated with Equation 3 without significant deviation, essentially decoupling the strain-hardening effects from the strain rate effects to give

(24)

Derivation of resistive force equations

For a rate-dependent target material, the axial force acting on the projectile nose after a change of variable is

(25)

Equation 25 requires the following set of integrals to be solved

(26)

(27)

(28)

(29)

By inspection, a general form of the set of integrals can be expressed as

(30)

Conical-nosed projectiles

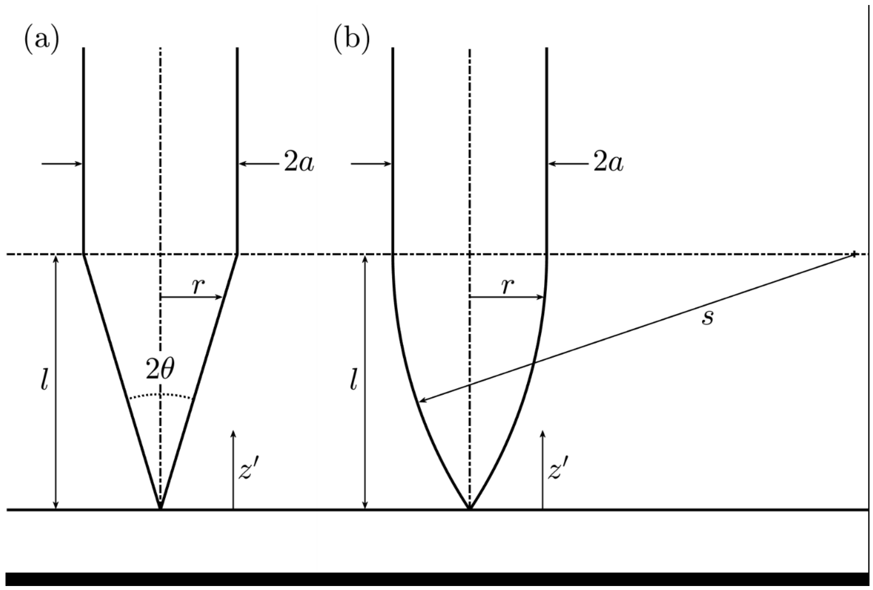

Figure 1: Dimensions of (a) conical-nosed and (b) ogival-nosed projectiles.

From Figure 1a, for a conical-nosed projectile with apex angle 2θ, . Solving the integrals in Equations 27 to 29, we get

(31)

Factoring out I_0 from Equation 26 and defining gives

(32)

(33)

(34)

Ogival-nosed projectile

From Figure 1b, for an ogival-nosed projectile

(35)

(36)

The variables , , and , where is the caliber-radius-head (CRH) of the projectile [5]. The special case of $m = 2$ for Equation 30 was solved by Forrestal & Warren [5] to give

(37a)

(b)

Unlike the conical-nosed projectile, the solution for I_β in this case requires numerical integration, since there is no generalized closed-form integral solution. Using exact solutions at = 1 and = N as fixed end constraints, a near-exact polynomial fit for can be obtained for numerical solutions to Equation 30 (Figure 2). can be evaluated with

(38)

The fit coefficients C_1 to C_4 for different caliber-radius-head values are given in Table I.

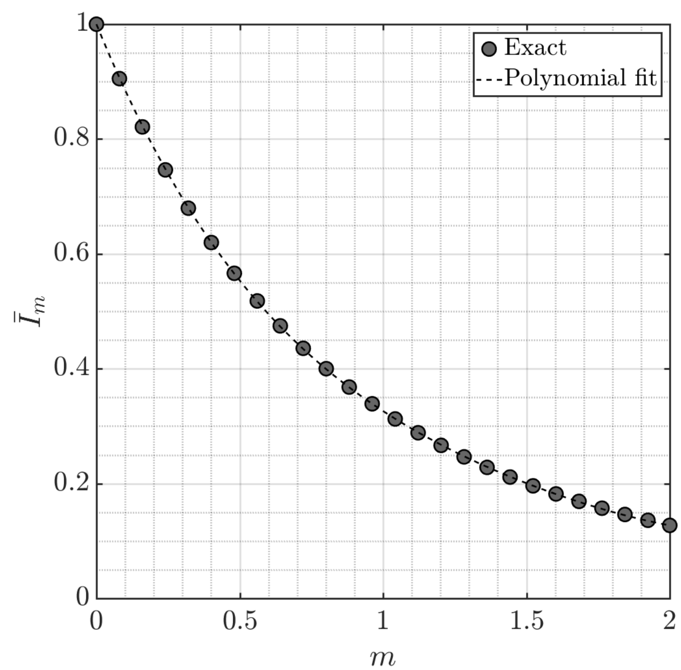

Figure 2: Polynomial fit of numerical solutions to integral for = 3.

Table I: Coefficients for different CRH values.

CRH	C_4	C_3	C_2	C_1
1	0.0171	-0.113	0.340	-0.590
2	0.0321	-0.211	0.599	-1.008
3	0.0453	-0.293	0.798	-1.225
4	0.0568	-0.361	0.953	-1.371
5	0.0668	-0.420	1.080	-1.481
6	0.0758	-0.471	1.187	-1.568

7	0.0838	-0.516	1.280	-1.641
8	0.0912	-0.557	1.362	-1.703
9	0.0979	-0.594	1.435	-1.757
10	0.1041	-0.628	1.501	-1.805

Solution with the rate-dependent force (Equation 32) for either nose geometry gives

(39)

Analytical solutions for Equation 39 again require numerical integration to calculate V_{bl}, since β is a real, non-integer value.

Numerical results

Numerical results for 6061-T6511 aluminum alloy are presented and compared to prior ballistic plate perforation data by Ryan et al. [10]. Warren and Forrestal [16] gave material properties for alloy 6061-T6511 as E = 68.9 GPa, ν = 0.33, Y = 276 MPa, ρ_t = 2710 kg/m^3, n = 0.072. The rate-sensitivity constants were obtained from prior studies across a broad range of strain rates [16], from quasi-static compression (10^{-3} s^{-1}) to pressure-shear experiments (10^5 s^{-1}). These values are reported as α = 32.0 MPa, β = 0.348 (given as m in reference), and = 1000 s^{-1}. The projectile is a 7.62-mm APM2 round with radius a = 3.93 mm and mass m_p = 10.8 g. The AP round has a CRH of approximately 3.0, giving N = 0.1272 and = 0.6589. Five variations of the CCE model are plotted in Figure 3 for comparison, and their respective sums of squared errors (SSE) are reported as follows:

I) Rate-independent (α = 0), no target inertia (C = 0), SSE = 1.59×10^6;
II) Rate-independent (α = 0), with target inertia, SSE = 4.04×10^5;
III) Rate-dependent, no target inertia (C = 0), SSE = 8.08×10^5;
IV) Rate-dependent, with target inertia, SSE = 1.67×10^5; and
V) Rate-independent (α = 0), no target inertia (C = 0), empirical fit (κ = 1.211), SSE = 1.33×10^5.

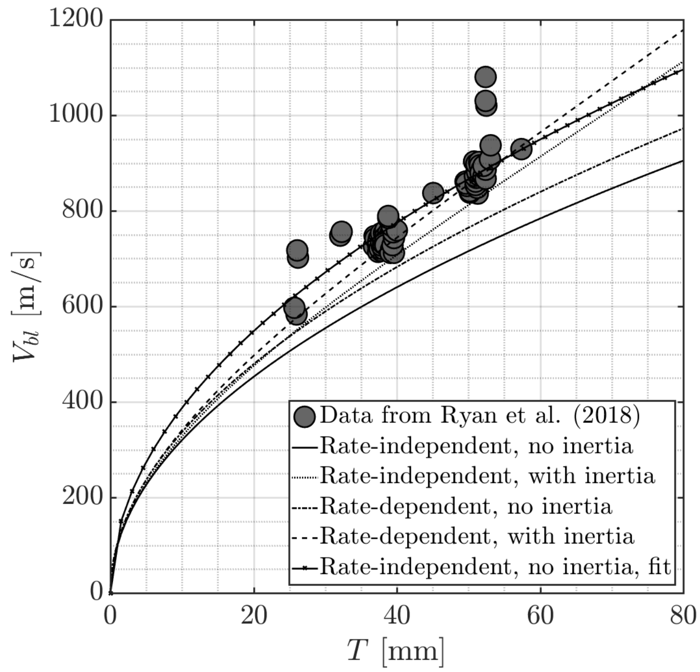

Figure 3: Variations of CCE model predictions for 7.62-mm APM2 round impacting 6061-T6511 aluminum alloy plates of different thicknesses.

The largest difference in ballistic performance appears to stem from target inertia effects, especially for much thicker targets, since C is a quadratic function of the target thickness. The rate-dependent model with inertia (Variation IV) provides the best prediction of the experimental data without empirically determined constants. It appears that ballistic performance predictions may be improved even though aluminum is often considered a relatively rate-insensitive material – this improvement in prediction may be true across the board for other more rate-sensitive materials.

Naturally, the empirically scaled rate-independent model (Equation 18, Variation V) in Figure 3 best fits the experimental data, as is the purpose of a least-squares fit. Such an empirical scaling has been previously used to model the plate perforation of AP rounds on an extensive range of aluminum alloys to great degrees of accuracy [6–11,22]. However, a comparison of Variations IV and V shows that the inclusion of rate effects results in a nonlinear response that cannot be linearly scaled, and such effects may be more pronounced for other materials that are considerably more rate-sensitive than aluminum.

Nonetheless, the frequent lack of experimental data across a broad range of strain rates to obtain the constants α and β for any target material has to be a consideration when including rate-sensitivity effects for ballistic performance prediction. Further work examining more rate-sensitive targets would provide further insight into the rate effects on the perforation dynamics in order to improve ballistic performance predictions.

Conclusions

Ballistic perforation equations for the rate-dependent cylindrical cavity expansion model were solved for conical- and ogival-nosed projectile geometries using material rate-sensitivity constants presented by Warren & Forrestal. Numerical results were presented for 7.62-mm APM2 rounds impacting relatively rate-insensitive 6061-T6511 aluminum alloy plates and compared with experimental ballistic impact data. The rate-dependent cavity expansion model was in good agreement with experimental data without the need for empirically determined constants, but simplified semi-empirical cavity expansion models derived with quasi-static properties provide an accurate performance prediction. This latter approach can be advantageous, as fewer material parameters are required for first order approximations.

Declaration of Competing Interest

The author(s) declare no known competing financial interests or personal relationships in the publication of this paper.

Acknowledgments

Work was supported through the INL Laboratory Directed Research & Development (LDRD) Program under DOE Idaho Operations Office Contract DE-AC07-05ID14517. Z.G. is also grateful to Dr. Michael J. Forrestal for the insightful discussions on his dynamic cavity expansion model.

References

[1] M.J. Forrestal, Z. Rosenberg, V.K. Luk, S.J. Bless, Perforation of Aluminum Plates With Conical-Nosed Rods, J. Appl. Mech. 54 (1987) 230–232. doi:10.1115/1.3172966.

[2] Z. Rosenberg, M.J. Forrestal, Perforation of Aluminum Plates with Conical-Nosed Rods—Additional Data and Discussion, J. Appl. Mech. 55 (1988) 236–238. doi:10.1115/1.3173639.

[3] M.J. Forrestal, V.K. Luk, N.S. Brar, Perforation of aluminum armor plates with conical-nose projectiles, Mech. Mater. 10 (1990) 97–105. doi:10.1016/0167-6636(90)90020-G.

[4] A.J. Piekutowski, M.J. Forrestal, K.L. Poormon, T.L. Warren, Perforation of aluminum plates with ogive-nose steel rods at normal and oblique impacts, Int. J. Impact Eng. 18 (1996) 877–887. doi:10.1016/S0734-743X(96)00011-5.

[5] M.J. Forrestal, T.L. Warren, Perforation equations for conical and ogival nose rigid projectiles into aluminum target plates, Int. J. Impact Eng. 36 (2009) 220–225. doi:10.1016/j.ijimpeng.2008.04.005.

[6] T. Børvik, M.J. Forrestal, T.L. Warren, Perforation of 5083-H116 Aluminum Armor Plates with Ogive-Nose Rods and 7.62 mm APM2 Bullets, Exp. Mech. 50 (2010) 969–978. doi:10.1007/s11340-009-9262-5.

[7] M.J. Forrestal, T. Børvik, T.L. Warren, Perforation of 7075-T651 Aluminum Armor Plates with 7.62 mm APM2 Bullets, Exp. Mech. 50 (2010) 1245–1251.

doi:10.1007/s11340-009-9328-4.
[8] M.J. Forrestal, T. Børvik, T.L. Warren, W. Chen, Perforation of 6082-T651 Aluminum Plates with 7.62 mm APM2 Bullets at Normal and Oblique Impacts, Exp. Mech. 54 (2013) 471–481. doi:10.1007/s11340-013-9817-3.
[9] S. Ryan, S.J. Cimpoeru, An evaluation of the Forrestal scaling law for predicting the performance of targets perforated in ductile hole formation, 3rd Int. Conf. Prot. Struct. (2015).
[10] S. Ryan, L.H. Nguyen, D. Gallardy, S.J. Cimpoeru, A scaling law for predicting the ballistic limit of aluminium alloy targets perforated in ductile hole formation, Int. J. Impact Eng. 116 (2018) 34–50. doi:10.1016/j.ijimpeng.2018.02.005.
[11] M.J. Forrestal, T.L. Warren, J.K. Holmen, Ballistic-Limit Velocities for 7.62 mm APM2 Bullets and Aluminum Alloy Armor Plates, J. Dyn. Behav. Mater. (2021). doi:10.1007/s40870-021-00313-8.
[12] Z. Guo, W. Chen, Dimensionless parameters for the perforation of ductile plates by armor-piercing rounds, Int. J. Impact Eng. 156 (2021) 103952. doi:10.1016/j.ijimpeng.2021.103952.
[13] M.J. Forrestal, K. Okajima, V.K. Luk, Penetration of 6061-T651 Aluminum Targets With Rigid Long Rods, J. Appl. Mech. 55 (1988) 755–760. doi:10.1115/1.3173718.
[14] M.J. Forrestal, V.K. Luk, Dynamic Spherical Cavity-Expansion in a Compressible Elastic-Plastic Solid, J. Appl. Mech. 55 (1988) 275. doi:10.1115/1.3173672.
[15] M.J. Forrestal, N.S. Brar, V.K. Luk, Penetration of Strain-Hardening Targets With Rigid Spherical-Nose Rods, J. Appl. Mech. 58 (1991) 7. doi:10.1115/1.2897183.
[16] T. Warren, M. Forrestal, Effects of strain hardening and strain-rate sensitivity on the penetration of aluminum targets with spherical-nosed rods, Int. J. Solids Struct. 35 (1998).
[17] T.L. Warren, The effect of strain rate on the dynamic expansion of cylindrical cavities, J. Appl. Mech. Trans. ASME. 66 (1999) 818–821. doi:10.1115/1.2791764.
[18] S. Skube, Large strain compression testing of ductile materials at quasi-static and dynamic strain rates, Purdue University, 2009.
[19] T. Børvik, M.J. Forrestal, O.S. Hopperstad, T.L. Warren, M. Langseth, Perforation of AA5083-H116 aluminium plates with conical-nose steel projectiles – Calculations, Int. J. Impact Eng. 36 (2009) 426–437. doi:10.1016/j.ijimpeng.2008.02.004.
[20] S. Yadav, D.R. Chichili, K.T. Ramesh, The mechanical response of a 6061-T6 A1/A12O3 metal matrix composite at high rates of deformation, Acta Metall. Mater. 43 (1995) 4453–4464. doi:10.1016/0956-7151(95)00123-D.
[21] J. Chakrabarty, Dynamic Plasticity, in: Appl. Plast., 2010. doi:10.1007/978-0-387-77674-3.
[22] M.J. Forrestal, B. Lim, W. Chen, A Scaling Law for APM2 Bullets and Aluminum Armor Plates, Exp. Mech. (2018). doi:10.1007/s11340-018-00442-7.